CORE
Metadata, citation and similar papers at core.ac.uk
Provided by Edinburgh Research Explorer

THE UNIVERSITY of EDINBURGH

Edinburgh Research Explorer

Signatures of thermal hysteresis in Tamm-wave propagation

Citation for published version:
Mackay, T 2017, 'Signatures of thermal hysteresis in Tamm-wave propagation' Journal of the Optical Society of America B, vol 34, no. 10, pp. 2155-2160. DOI: 10.1364/JOSAB.34.002155

Digital Object Identifier (DOI):
10.1364/JOSAB.34.002155

Link:
Link to publication record in Edinburgh Research Explorer

Document Version:
Early version, also known as pre-print

Published In:
Journal of the Optical Society of America B

General rights
Copyright for the publications made accessible via the Edinburgh Research Explorer is retained by the author(s) and / or other copyright owners and it is a condition of accessing these publications that users recognise and abide by the legal requirements associated with these rights.

Take down policy
The University of Edinburgh has made every reasonable effort to ensure that Edinburgh Research Explorer content complies with UK legislation. If you believe that the public display of this file breaches copyright please contact openaccess@ed.ac.uk providing details, and we will remove access to the work immediately and investigate your claim.

OPEN ACCESS

Download date: 30. Jun. 2018

Signatures of thermal hysteresis in Tamm-wave propagation

Francesco Chiadini[1], Vincenzo Fiumara[2], Tom G. Mackay[3,4], Antonio Scaglione[1], and Akhlesh Lakhtakia[4]

[1]Department of Industrial Engineering, University of Salerno, via Giovanni Paolo II, 132 – Fisciano (SA), 84084, Italy;

[2]School of Engineering, University of Basilicata, Viale dell'Ateneo Lucano 10, 85100 Potenza, Italy;

[3]School of Mathematics and Maxwell Institute for Mathematical Sciences, University of Edinburgh, Edinburgh EH9 3FD, UK;

[4]Department of Engineering Science and Mechanics, Pennsylvania State University, University Park, PA 16802–6812, USA

arXiv:1709.08722v1 [physics.optics] 25 Sep 2017

Abstract

We numerically solved the boundary-value problem for Tamm waves (which may also be classified as Uller–Zenneck waves here) guided by the planar interface of a homogeneous isotropic dissipative dielectric (HIDD) material and a periodically multilayered isotropic dielectric material. The HIDD material was chosen to be VO_2 which, at optical wavelengths, has a temperature-dependent refractive index with a hysteresis feature, i.e., the temperature-dependence of its refractive index varies depending upon whether the temperature is increasing or decreasing. A numerical code was implemented to extract solutions of the dispersion equation at a fixed wavelength for both p- and s-polarization states over the temperature range $[50, 80]$ °C. A multitude of Tamm waves of both linear polarization states were found, demonstrating a clear demarcation of the heating and cooling phases in terms of wavenumbers and propagation distances. Thereby, the signatures of thermal hysteresis in Tamm-wave propagation were revealed.

1 Introduction

An electromagnetic surface wave (ESW) can be guided by the planar interface of two different materials [1, 2]. Various types of ESWs can occur whose classifications and characteristics are determined by the materials forming the interface [3]. Included in these types are Tamm waves and Uller–Zenneck waves.

Tamm waves are ESWs guided by the planar interface of two isotropic dielectric materials, one of them being periodically inhomogeneous in the direction normal to the interface. The existence of Tamm waves has been predicted theoretically [4] and established experimentally [5], and these ESWs have been harnessed for optical-sensing applications [6–9].

Uller-Zenneck waves are ESWs guided by the planar interface of two dielectric materials, one of which is required to be dissipative. The existence of Uller-Zenneck waves was predicted theoretically in the early years of the twentieth century [10–14], but unambiguous experimental confirmation was only provided very recently [15].

In this paper we solve the canonical boundary-value problem of ESWs guided by the planar interface of two isotropic dielectric materials, one of which is periodically inhomogeneous in the direction normal to the interface and the other is a dissipative material. The ESWs under consideration may be classified as either Tamm waves or Uller–Zenneck waves; for definiteness, the former classification is chosen here.

The numbers and propagation characteristics of such ESWs are determined by the structural and constitutive properties of the two partnering materials on either side of the interface. As an example, the periodicity of one of the two partnering materials may determine the number of the ESWs that can be excited [16]. Furthermore, if a partnering material has temperature-sensitive constitutive properties, then the number and propagation characteristics of ESWs may be controlled by varying the temperature; indeed, Dyakonov surface waves may be converted to surface–plasmon–polariton waves by increasing the temperature, for example [17].

For the partnering material that is a homogeneous isotropic dissipative dielectric (HIDD) material we chose VO_2 which, at optical wavelengths, has a temperature-dependent refractive index n_d [18] with a hysteresis [19] feature, i.e., the temperature-dependence of n_d varies depending upon whether the temperature is increasing or decreasing. For the periodically nonhomogeneous partnering material, we chose a periodic multilayered isotropic dielectric (PMLID) material, comprising layers of alloys of silicon oxide and silicon nitride, whose refractive indexes were assumed to be insensitive to temperature over the range $[50, 80]$ °C for the near-infrared regime. The PMLID material is nondissipative.

The goal of our study is to delineate the signatures of thermal hysteresis in Tamm-wave propagation. The paper is organized as follows: in Sec. 2 the canonical boundary-value problem for ESW propagation guided by the planar HIDD/PMLID interface is presented. In Sec. 3 numerical results highlighting the signatures of thermal hysteresis in Tamm-wave propagation, at a fixed free-space wavelength $\lambda_0 = 800$ nm, are reported and discussed for both p- and s-polarization states. Conclusions follow in Sec. 4.

2 Theoretical Preliminaries and Materials

In this section we present the formulation of the boundary-value problem, wherein the half space $z \leq 0$ is occupied by a HIDD material with complex refractive index n_d, and the half space $z \geq 0$ is occupied by a PMLID material. A schematic representation of the boundary-value problem is provided in Fig. 1.

The HIDD material was taken to be VO_2 whose refractive index n_d in the range $[50, 80]$ °C is a function of temperature, with a thermal hysteresis feature. The thermal hysteresis of VO_2 has been quantified by Cormier *et al.* for the near-infrared regime [18], and is illustrated in Fig. 2. Specifically, n_d in the range $[50, 80]$ °C shows two different dependencies on temperature: one for heating the material from 50 to 80 °C and the other for cooling the material from 80 to 50 °C. As shown in Fig. 2, graphs of both the real and imaginary parts of n_d plotted against temperature exhibit the typical hysteresis shape (as arises for plots of magnetization versus magnetic field in the case of magnetic hysteresis [19], for example)

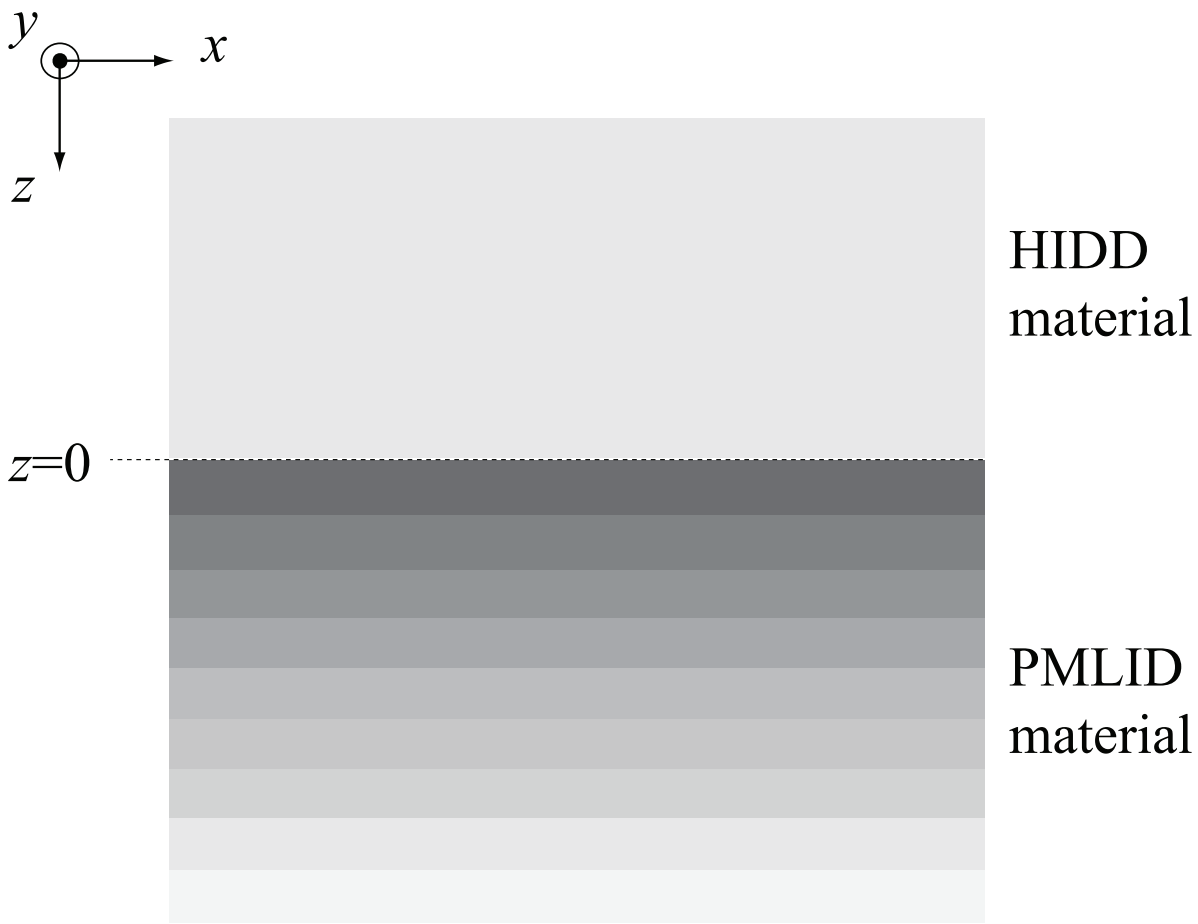

Figure 1: Schematic representation of the canonical boundary-value problem.

Table 1: **Refractive index n_j of the dielectric layers j in the unit cell of the PMLID material at $\lambda_0 = 800$ nm.**

j	n_j
1	1.9656
2	1.8062
3	1.7650
4	1.7243
5	1.6518
6	1.6105
7	1.5590
8	1.5174
9	1.4748

with the heating graph (dashed red curve) lying above the cooling graph (solid blue curve) for the real part of n_d and lying below for the imaginary part of n_d.

The unit cell of the PMLID material is constructed from 9 lossless dielectric layers. Each layer is an alloy of silicon oxide and silicon nitride, the proportion of these being different for each layer [20]. The sequence of the values of the refractive index n_j ($j = 1, ..., 9$) in the unit cell of the PMLID material is shown in Table 1, where the layer numbered $j = 1$ has the lowest value of the Cartesian coordinate z. Each layer has a thickness of 75 nm.

As both partnering materials are isotropic, the canonical boundary-value problem can be partitioned into two independent problems, one for p-polarized Tamm waves and the other for s-polarized Tamm waves. Let the Cartesian unit vectors be identified as $\mathbf{u}_x$, $\mathbf{u}_y$, and $\mathbf{u}_z$. Without loss of generality, we consider Tamm waves propagating parallel to the unit vector $\mathbf{u}_x$. The amplitude of any ESW is required to decay as $z \to \pm\infty$. With q as the generally complex-valued wavenumber, the electric and magnetic field phasors can be represented everywhere as

$$\left.\begin{aligned} \mathbf{E}(\mathbf{r}) &= [e_x(z)\mathbf{u}_x + e_z(z)\mathbf{u}_z]\exp(iqx) \\ \mathbf{H}(\mathbf{r}) &= h_y(z)\mathbf{u}_y \exp(iqx) \end{aligned}\right\}, \quad z \in (-\infty, \infty)\,, \tag{1}$$

for the p-polarized Tamm waves, and as

$$\left.\begin{aligned} \mathbf{E}(\mathbf{r}) &= e_y(z)\mathbf{u}_y \exp(iqx) \\ \mathbf{H}(\mathbf{r}) &= [h_x(z)\mathbf{u}_x + h_z(z)\mathbf{u}_z]\exp(iqx) \end{aligned}\right\}, \quad z \in (-\infty, \infty)\,, \tag{2}$$

for the s-polarized Tamm waves, where $e_x(z)$, $e_z(z)$, and $h_y(z)$ and $e_y(z)$, $h_x(z)$, and $h_z(z)$ are unknown functions. For the p- and s-polarized Tamm waves, labeled by the subscript $\ell \in \{p, s\}$, the dispersion equation which determines the wavenumber q can be written as

$$\det\{\underline{\underline{M}}_\ell(q)\} = 0\,, \qquad \ell \in \{p, s\}\,, \tag{3}$$

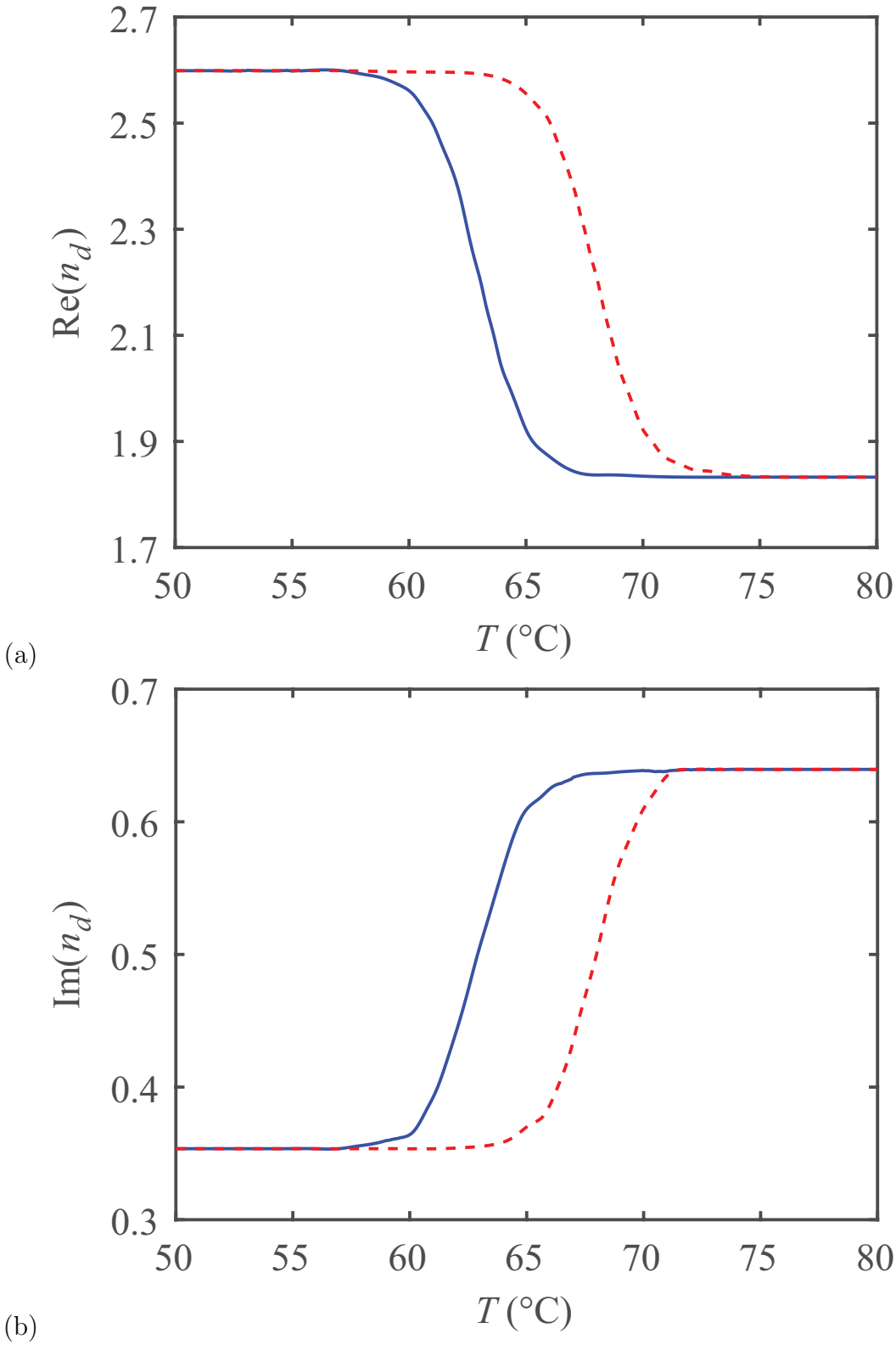

Figure 2: (Color online) Refractive index of VO_2 at $\lambda_0 = 800$ nm as a function of temperature (in degree Celsius): (a) real part of n_d; (b) imaginary part of n_d. Solid (blue) curve: cooling phase; dashed (red) curve: heating phase.

where $\underline{\underline{M}}_\ell$ is a 2×2 matrix with functional dependence on q, whose derivation is described in detail elsewhere [21]. A numerical code was developed to extract wavenumbers q from (3). The propagation distance — i.e., the distance along the direction of propagation $\mathbf{u}_x$ over which the fields reduce by a factor of $\exp(-1) = 0.367$, and the power density reduces by a factor of $\exp(-2) = 0.135$ — is calculated from the imaginary part of q as $\Delta_{prop} = 1/\mathrm{Im}(q)$. We also define the normalized wavenumber $\tilde{q} = q/k_0$, where $k_0 = 2\pi/\lambda_0$ is the free-space wavenumber.

3 Numerical Results and Discussions

At a fixed free-space wavelength $\lambda_0 = 800$ nm, (3) was numerically solved with the temperature varying over the range $[50, 80]$ °C. At each temperature, multiple solutions of (3) exist. These solutions can be organized in branches with respect to temperature variation.

Owing to the large number of solution branches, it is convenient to present the solution branches in three groups for each polarization state:

(i) plots of $\mathrm{Re}(\tilde{q})$ and Δ_{prop} as the temperature increases from 50 °C to 80 °C (red dashed curves) and decreases from 80 °C to 50 °C (blue solid curves) for solution branches with $\mathrm{Re}(\tilde{q}) > 1$ at $T = 50$ °C are presented in Figs. 3 and 4 for p-polarized Tamm waves and in Figs. 5 and 6 for s-polarized Tamm waves;

(ii) plots of $\mathrm{Re}(\tilde{q})$ and Δ_{prop} as the temperature increases from 50 °C to 80 °C (red dashed curves) and decreases from 80 °C to 50 °C (blue solid curves) for solution branches with $0.1 < \mathrm{Re}(\tilde{q}) < 1$ at $T = 50$ °C are presented in Figs. 7 and 8 for p-polarized Tamm waves and in Figs. 9 and 10 for s-polarized Tamm waves; and

(iii) plots of $\mathrm{Re}(\tilde{q})$ and Δ_{prop} as the temperature increases from 50 °C to 80 °C (red dashed curves) and decreases from 80 °C to 50 °C (blue solid curves) for solution branches with $0.01 < \mathrm{Re}(\tilde{q}) < 0.1$ at $T = 50$ °C are presented in Figs. 11 and 12 for p-polarized Tamm waves and in Figs. 13 and 14 for s-polarized Tamm waves.

In each of Figs. 3–14 there is a clear distinction between the heating and cooling phases. This distinction — which arises for both p-polarized and s-polarized Tamm waves — reflects hysteresis in the temperature dependence of the refractive index of VO_2 for the heating and cooling phases. Each pair of heating and cooling curves can be classified as either of signature A or of B, as follows:

Signature A: The extremum value of $\mathrm{Re}(\tilde{q})$ is approximately the same in both heating and cooling phases, but it occurs at different temperatures in the two phases. Plots of Δ_{prop} for the heating and cooling phases exhibit the typical hysteresis shape [19]. The hysteresis shape depends on whether Δ_{prop} at $T = 50$ °C is greater or smaller than its value at $T = 80$ °C. Thus, signature A can be divided into two subsignatures:

Subsignature Aa: Δ_{prop} at $T = 50$ °C is smaller than its value at $T = 80$ °C , and

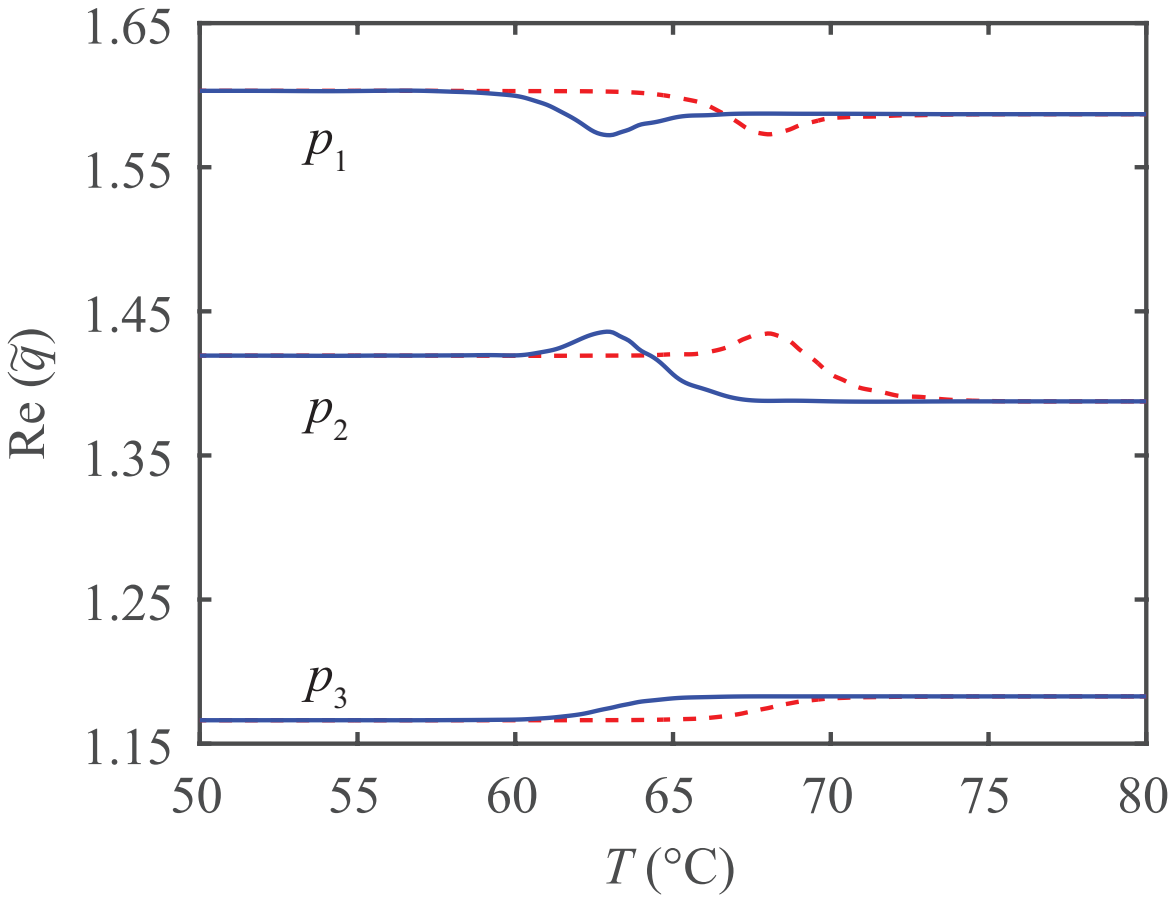

Figure 3: (Color online) Re($\tilde{q}$) versus temperature for p-polarized Tamm waves for which Re($\tilde{q}$)> 1 at $T = 50$ °C. Solid (blue) curve: cooling phase; dashed (red) curve: heating phase.

Subsignature Ab: Δ_{prop} at $T = 50$ °C is larger than its value at $T = 80$ °C.

Signature B: The extremum value of Δ_{prop} is approximately the same in both heating and cooling phases, but occurs at different temperatures in the two phases. Plots of Re($\tilde{q}$) for the heating and cooling phases exhibit the typical hysteresis shape [19]. For all solutions branches of signature B, Re($\tilde{q}$) at $T = 50$ °C is smaller than its value at $T = 80$ °C.

In order to illustrate the foregoing classification, representative hysteresis shapes for the signatures Aa, Ab, and B are identified in Table 2.

Figures 3 and 4 illustrate Re($\tilde{q}$) and Δ_{prop}, respectively, for p-polarized Tamm waves when Re($\tilde{q}$)> 1. The solutions are organized in three branches labeled p_1 to p_3. The branch p_1 is of signature Aa, branch p_2 is of signature Ab, while branch p_3 is of signature B. Figures 5 and 6 depict Re($\tilde{q}$) and Δ_{prop}, respectively, for s-polarized Tamm waves when Re($\tilde{q}$)> 1. In these figures the solutions are organized in two branches labeled s_1 and s_2. Both branches are of signature B.

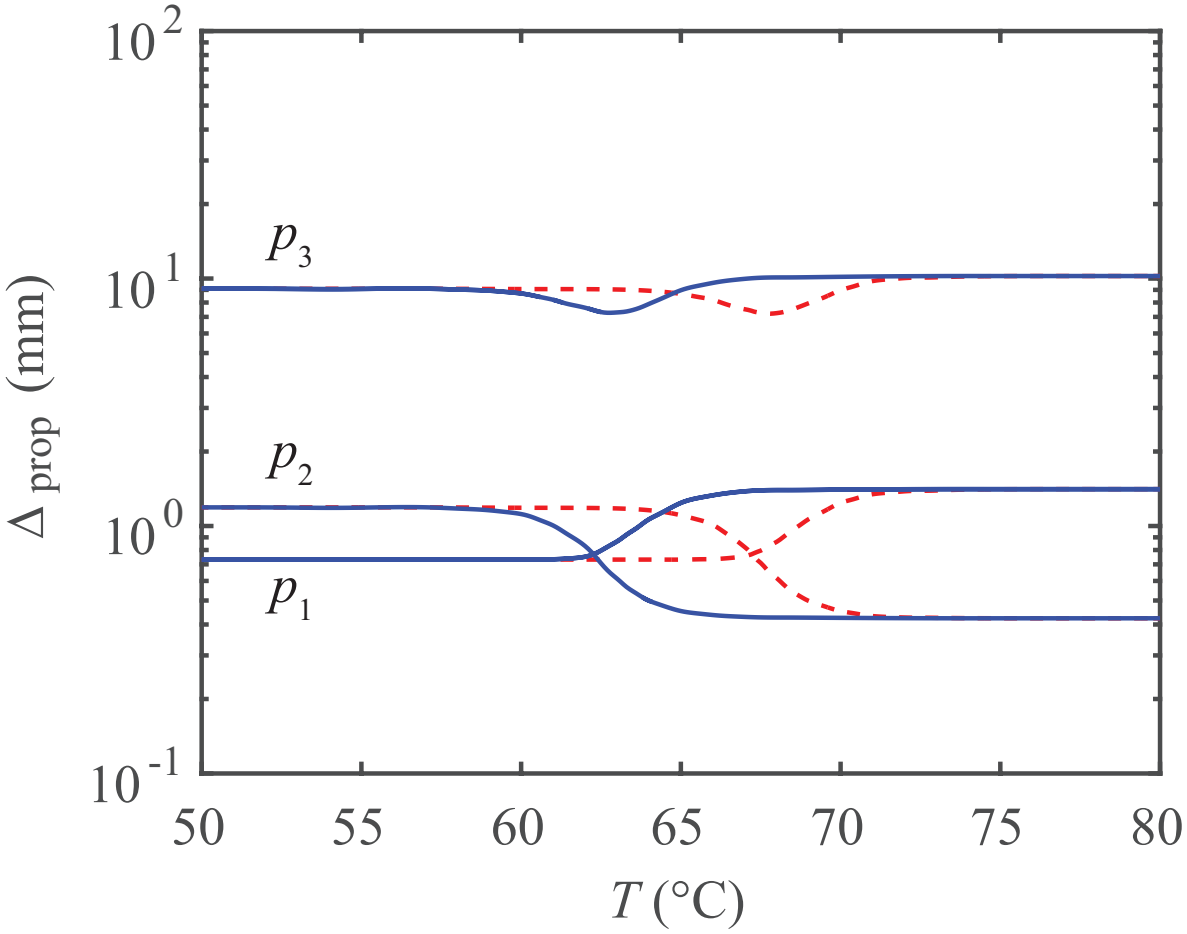

Figure 4: (Color online) Δ_{prop} versus temperature for p-polarized Tamm waves for which $\mathrm{Re}(\tilde{q})> 1$ at $T = 50$ °C. Solid (blue) line: cooling phase; dashed (red) line: heating phase.

Figures 7 and 8 illustrate $\mathrm{Re}(\tilde{q})$ and Δ_{prop}, respectively, for p-polarized Tamm waves when $\mathrm{Re}(\tilde{q})$ at $T = 50$ °C takes a value greater than 0.1 and less than 1. The solutions are organized in two branches labeled p_4 and p_5. Both branches are of signature Aa. Figures 9 and 10 depict $\tilde{q}$ and Δ_{prop} for s-polarized Tamm waves when $\mathrm{Re}(\tilde{q})$ at $T = 50$ °C takes a value between 0.1 and 1. The solitary solution represented in these figures, labeled s_3, is of signature Aa.

Figures 11 and 12 illustrate $\mathrm{Re}(\tilde{q})$ and Δ_{prop}, respectively, for p-polarized Tamm waves when $\mathrm{Re}(\tilde{q})$ at $T = 50$ °C takes a value between 0.01 and 0.1. The solutions are organized in twelve branches labeled from p_6 to p_{17} in descending order with respect to the $\mathrm{Re}(\tilde{q})$ values at $T = 50$ °C. Solution branches in Fig. 11 have rather similar $\mathrm{Re}(\tilde{q})$ values and their graphs cross each other. In contrast, the Δ_{prop} graphs of the $p_6 - p_{17}$ solution branches do not intersect each other. The typical hysteresis shape can be recognized for most of the Δ_{prop} graphs. All solution branches from p_6 to p_{17} are of signature Aa. Figures 13 and 14 depict $\tilde{q}$ and Δ_{prop}, respectively, for the s-polarization state when $\mathrm{Re}(\tilde{q})$ at $T = 50$ °C takes a value

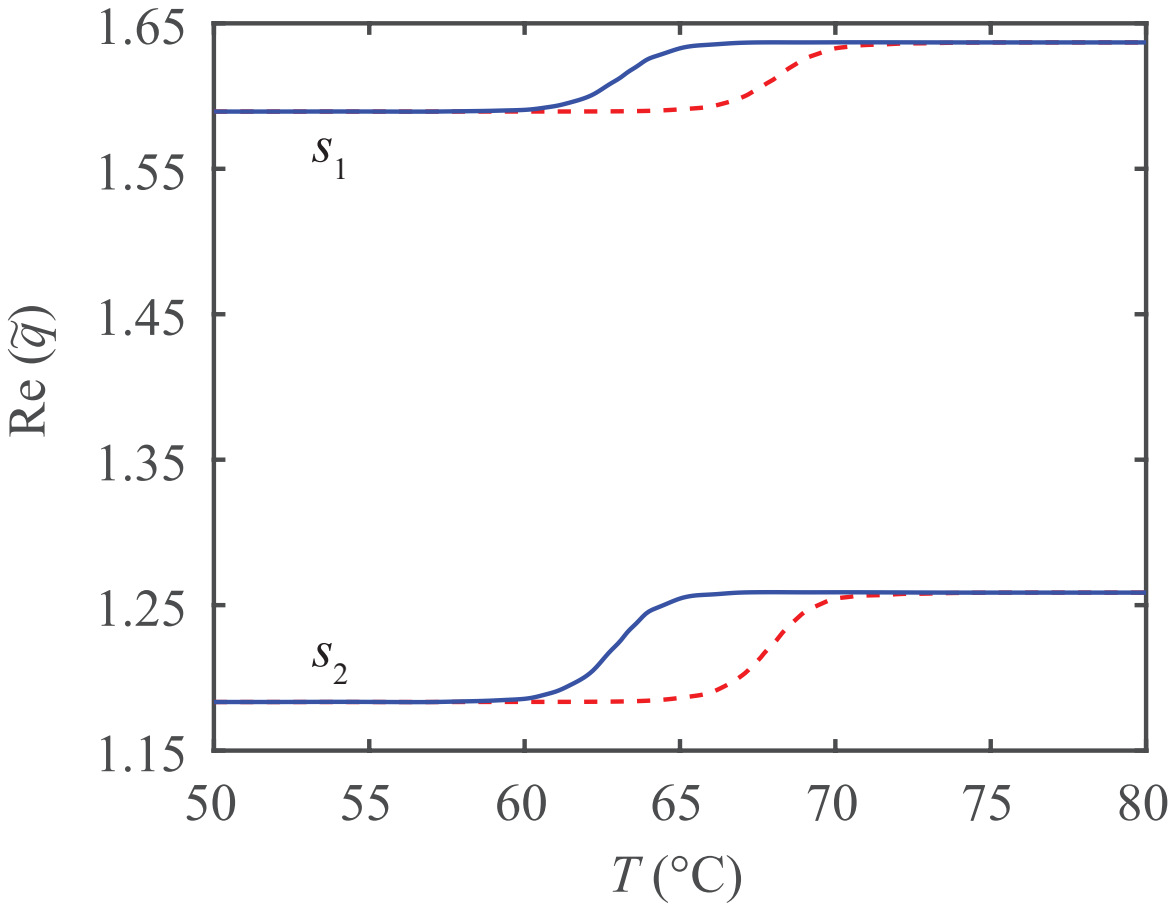

Figure 5: As Fig. 3 but for s-polarized Tamm waves.

between 0.01 and 0.1. The solutions are organized in twelve branches labeled from s_4 to s_{15} in descending order with respect to the Re($\tilde{q}$) values at $T = 50$ °C. All the remarks made for the p-polarization state represented in Figs. 11 and 12 also hold for the s-polarization state represented in Figs. 13 and 14. Thus, all branch solutions from s_5 to s_{15} are of signature Aa.

When Re($\tilde{q}$)< 0.01 at $T = 50$ °C, for both polarization states, a multitude of solutions were found with Re($\tilde{q}$) values that are very small and very close to each other. These solutions are not presented graphically here as the corresponding graphs are practically indistinguishable from each other. It is worth noting that for solutions with very small Re($\tilde{q}$) values, the values of Im($\tilde{q}$) are very high which results in tiny values of Δ_{prop}. The corresponding Tamm waves can therefore be identified as local ESWs. Finding these solutions is numerically challenging because extremely high resolution is needed. As a consequence, for Re($\tilde{q}$)$< 10^{-4}$ our code is not able to reliably determine solutions.

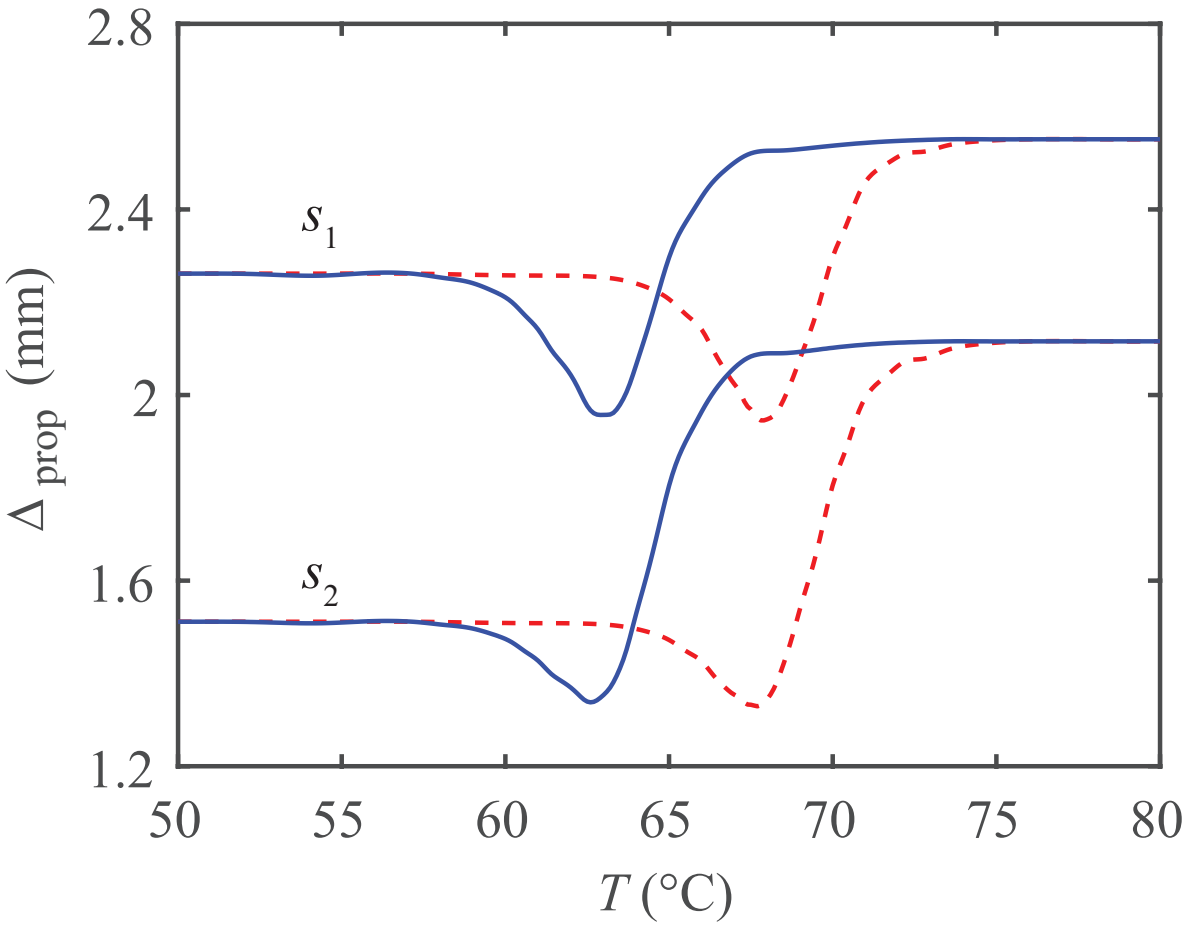

Figure 6: As Fig. 4 but for s-polarized Tamm waves.

4 Concluding remarks

We numerically solved the boundary-value problem for Tamm waves (which may be alternatively classified as Uller–Zenneck waves) guided by the interface of a homogeneous isotropic dissipative dielectric material and a periodic multilayered isotropic dielectric material. The HIDD material was chosen to have a temperature-dependent refractive index with a hysteresis feature. A numerical code was developed to extract solutions of the dispersion equation at a fixed wavelength for Tamm waves of both p- and s-polarization states. A multitude of Tamm waves exist of both p- and s-polarization states which show a clear distinction between heating and cooling phases, reflecting the temperature-dependence of the refractive index of the HIDD material for the two phases. Thus, the signatures of thermal hysteresis in Tamm-wave propagation were revealed. Parenthetically, the physical significance and applicability of our study are bolstered by the fact that experimental data has been used for the relative permittivity of VO_2 as well as of SiO_2–SiN_2 alloys of nine different compositions.

Table 2: **Representative hysteresis shapes.**

Solution signature	$\mathrm{Re}(\tilde{q})$	Δ_{prop}
Aa	no typical hysteresis shape	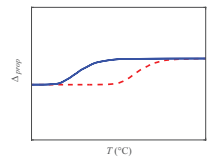
Ab	no typical hysteresis shape	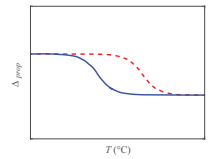
B	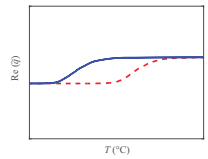	no typical hysteresis shape

Acknowledgment. AL thanks the Charles Godfrey Binder Endowment at Penn State for ongoing support of his research.

References

[1] A. D. Boardman, *Electromagnetic Surface Modes*, (Wiley, New York, NY, USA, 1982).

[2] J. A. Polo Jr., T. G. Mackay, and A. Lakhtakia, *Electromagnetic Surface Waves: A Modern Perspective* (Elsevier, Waltham, MA, USA, 2013).

[3] F. Chiadini, V. Fiumara, A. Scaglione A., and A. Lakhtakia, "Compound guided waves that mix characteristics of surface-plasmon-polariton, Tamm, Dyakonov–Tamm, and Uller–Zenneck waves," J. Opt. Soc. Am. B **33**, 1197–1206 (2016).

[4] P. Yeh, A. Yariv, and C.-S. Hong, "Electromagnetic propagation in periodic stratified media. I. General theory," J. Opt. Soc. Am. **67**, 423–438 (1977).

[5] P. Yeh, A. Yariv, and A. Y. Cho, "Optical surface waves in periodic layered media," Appl. Phys. Lett. **32**, 104–105 (1978).

[6] M. Shinn and W. M. Robertson, "Surface plasmon-like sensor based on surface electromagnetic waves in a photonic band-gap material" Sens. Actuat. B: Chem. **105**, 360–364 (2005).

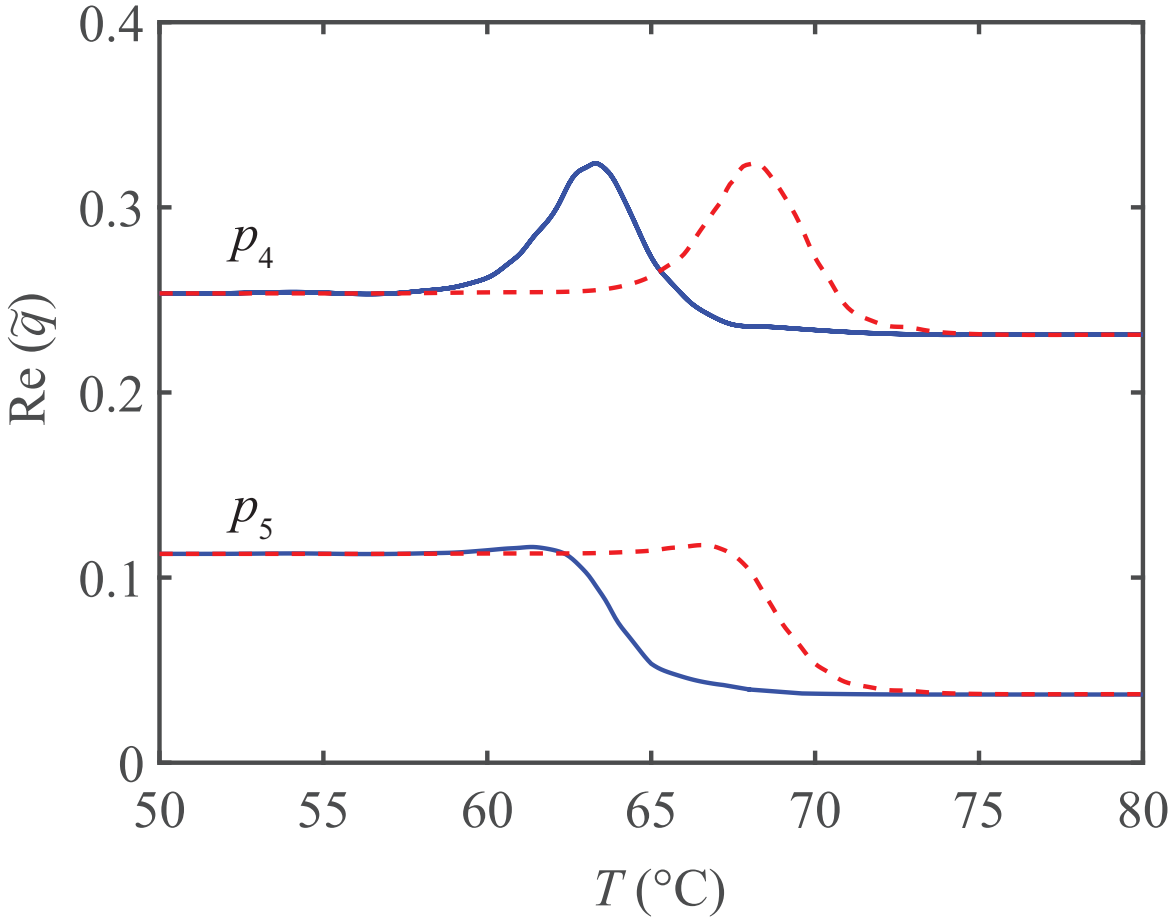

Figure 7: As Fig. 3 but for 0.1 <Re($\tilde{q}$)< 1 at $T = 50$ °C.

[7] V. N. Konopsky and E. V. Alieva, "Photonic crystal surface waves for optical biosensors," Anal. Chem. **79**, 4729–4735 (2007).

[8] A. Sinibaldi, N. Danz, E. Descrovi, P. Munzert, U. Schulz, F. Sonntag, L. Dominici, and F. Michelotti, "Direct comparison of the performance of Bloch surface wave and surface plasmon polariton sensors," Sens. Actuat. B: Chem. **174**, 292–298 (2012).

[9] V. N. Konopsky, T. Karakouz, E. V. Alieva, C. Vicario, S. K. Sekatskii, and G. Dietler, "Photonic crystal biosensor based on optical surface waves," Sensors **13**, 2566–2578 (2013).

[10] K. Uller *Beiträge zur Theorie der Elektromagnetischen Strahlung,* Ph.D. thesis (Rostock, Germany: Universität Rostock), Chap. XIV, 1903.

[11] J. Zenneck, "Über die Fortpflanzung ebener elektromagnetischer Wellen längs einer ebenen Lieterfläche und ihre Beziehung zur drahtlosen Telegraphie," Ann. Phys. Lpz. **23**, 846–866 (1907).

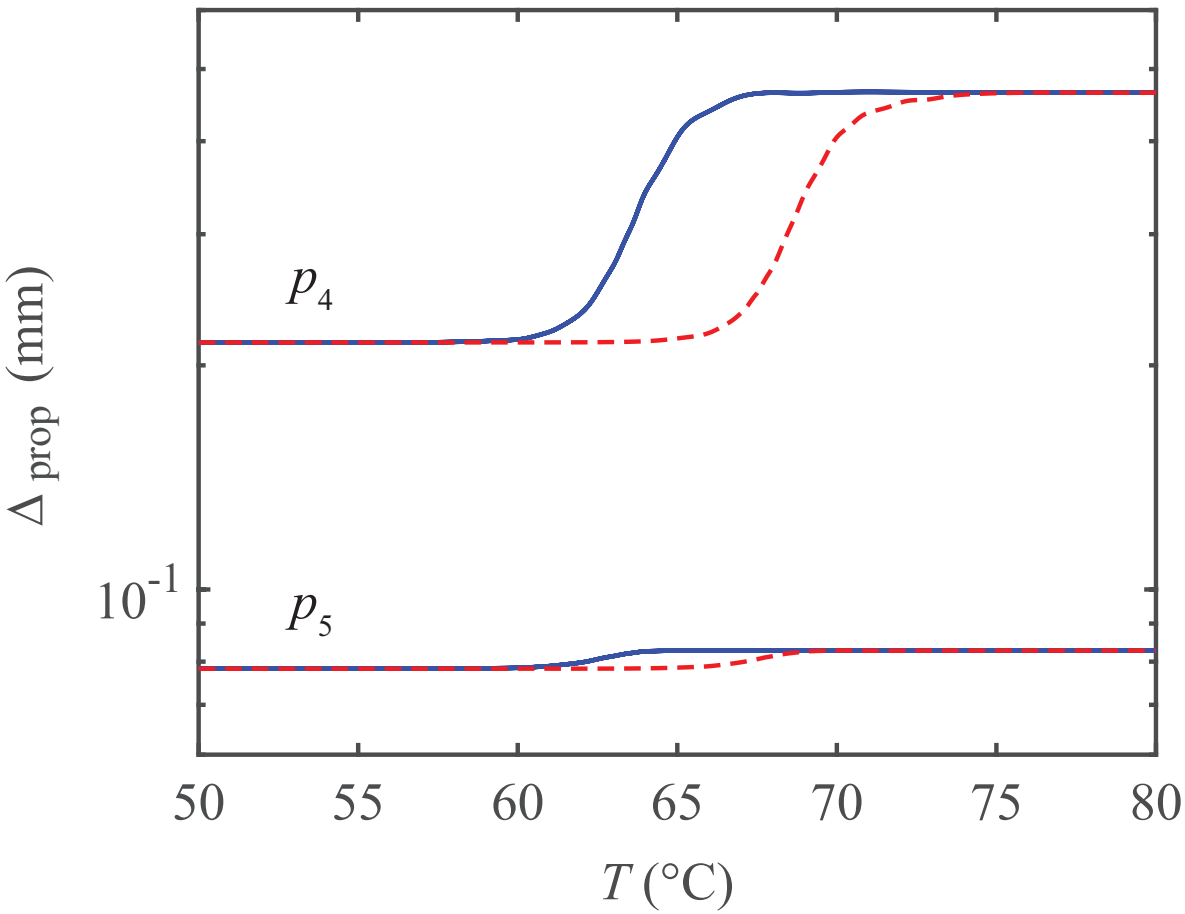

Figure 8: As Fig. 4 but for 0.1 <Re($\tilde{q}$)< 1 at $T = 50$ °C.

[12] A. Sommerfeld, "Über die Ausbreitung der Wellen in der drahtlosen Telegraphie," Ann. Phys. Lpz. **28**, 665–736 (1909).

[13] A. Sommerfeld, "Über die Ausbreitung der Wellen in der drahtlosen Telegraphie," Ann. Phys. Lpz. **62**, 95–96 (1920).

[14] A. Sommerfeld, "Über die Ausbreitung der Wellen in der drahtlosen Telegraphie," Ann. Phys. Lpz. **81**, 1135–1153 (1926).

[15] M. Faryad and A. Lakhtakia, "Observation of the Uller–Zenneck wave," Opt. Lett. **39**, 5204–5207 (2014).

[16] F. Chiadini, V. Fiumara, A. Scaglione, and A. Lakhtakia, "Periodicity effects on compound waves guided by a thin metal slab sandwiched between two periodically nonhomogeneous dielectric materials," J. Nanophoton. **11**, 043507 (2017).

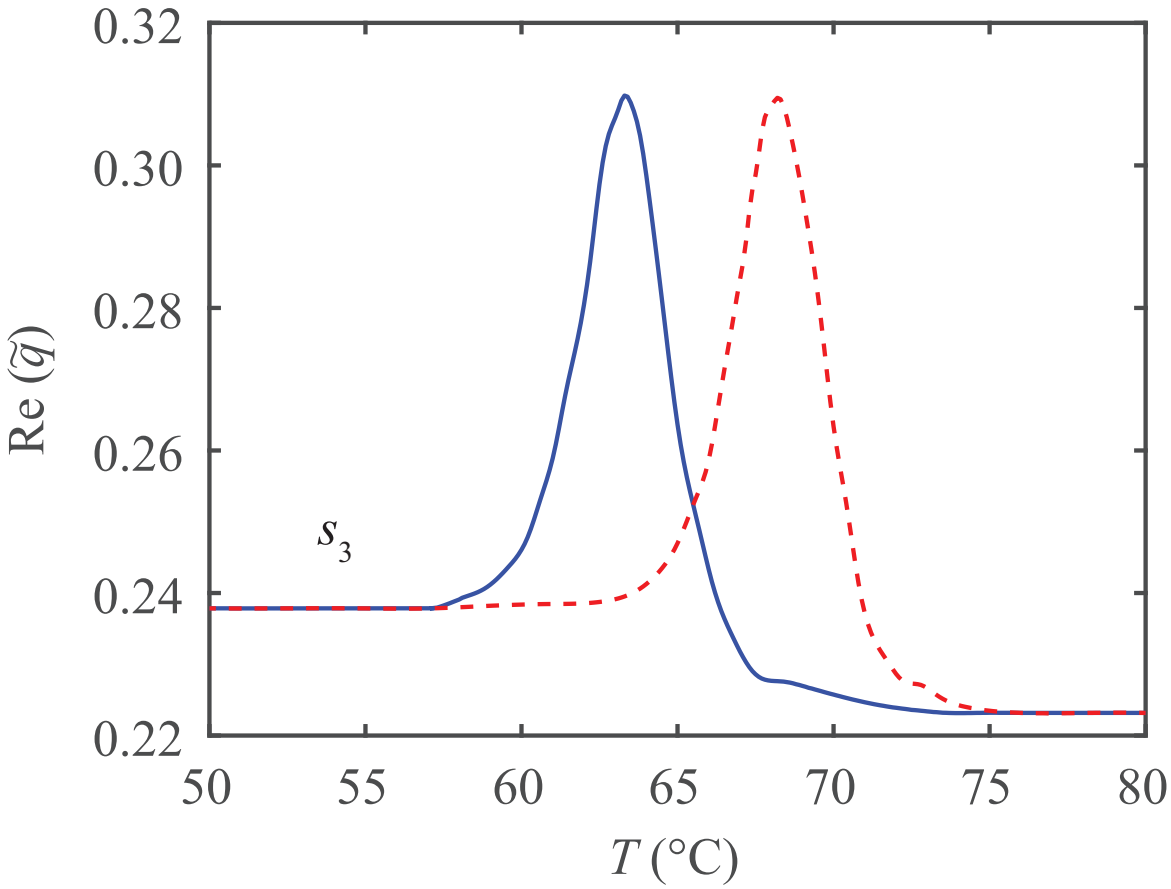

Figure 9: As Fig. 5 but for 0.1 <Re($\tilde{q}$)< 1 at $T = 50$ °C.

[17] F. Chiadini, V. Fiumara, T. G. Mackay, A. Scaglione, and A. Lakhtakia, "Temperature-mediated transition from Dyakonov–Tamm surface waves to surface-plasmon-polariton waves," J. Opt. (UK) **19**, 085002 (2017).

[18] P. Cormier, T. V. Son, J. Thibodeau, A. Doucet, V.-V. Truong, and A. Haché, "Vanadium dioxide as a material to control light polarization in the visible and near infrared," Opt. Commun. **382**, 80–85 (2017).

[19] S. Chikazumi, *Physics of Ferromagnetism, 2nd Ed.* (Clarendon Press, Oxford, UK, 1997).

[20] M. Faryad, A. S. Hall, G. D. Barber, T. E. Mallouk, and A. Lakhtakia, "Excitation of multiple surface-plasmon-polariton waves guided by the periodically corrugated interface of a metal and a periodic multilayered isotropic dielectric material," J. Opt. Soc. Am. B **29**, 704–713 (2012).

[21] F. Chiadini, V. Fiumara, A. Scaglione, and A. Lakhtakia, "Composite surface-plasmon-polariton waves guided by a thin metal layer sandwiched between a homogeneous

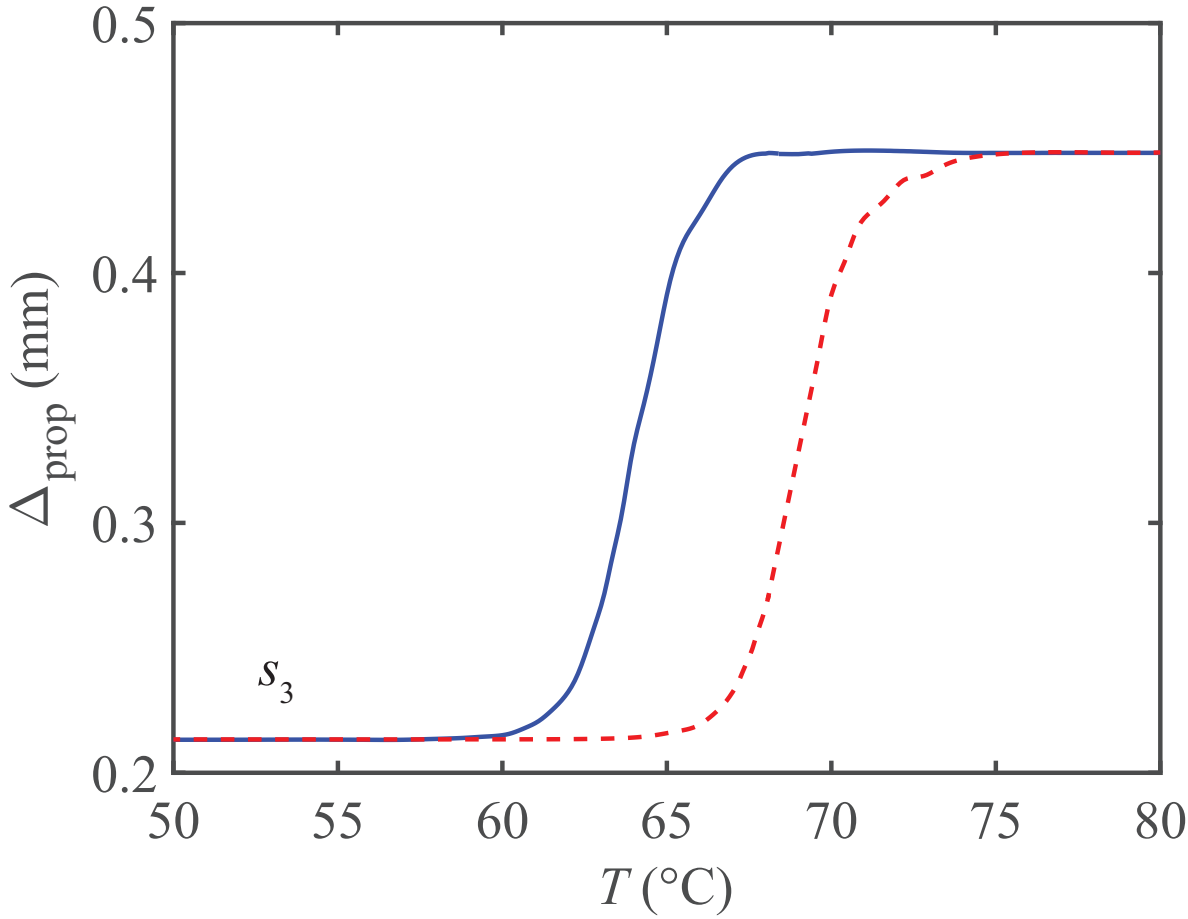

Figure 10: As Fig. 6 but for 0.1 <Re($\tilde{q}$)< 1 at $T = 50$ °C.

isotropic dielectric material and a periodically multilayered isotropic dielectric material," J. Nanophoton. **9**, 093060 (2015).

[22] H. Maab, M. Faryad, and A. Lakhtakia, "Surface electromagnetic waves supported by the interface of two semi-infinite rugate filters with sinusoidal refractive-index profiles," J. Opt. Soc. Am. B **28**, 204–1212 (2011).

[23] A. Kavokin, I. Shelykh, and G. Malpuech, "Lossless interface modes at the boundary between two periodic dielectric structures," Phys. Rev. B **72**, 233102 (2005).

[24] A. Kavokin, I. Shelykh, and G. Malpuech, "Optical Tamm states for the fabrication of polariton lasers," Appl. Phys. Lett. **87**, 261105 (2005).

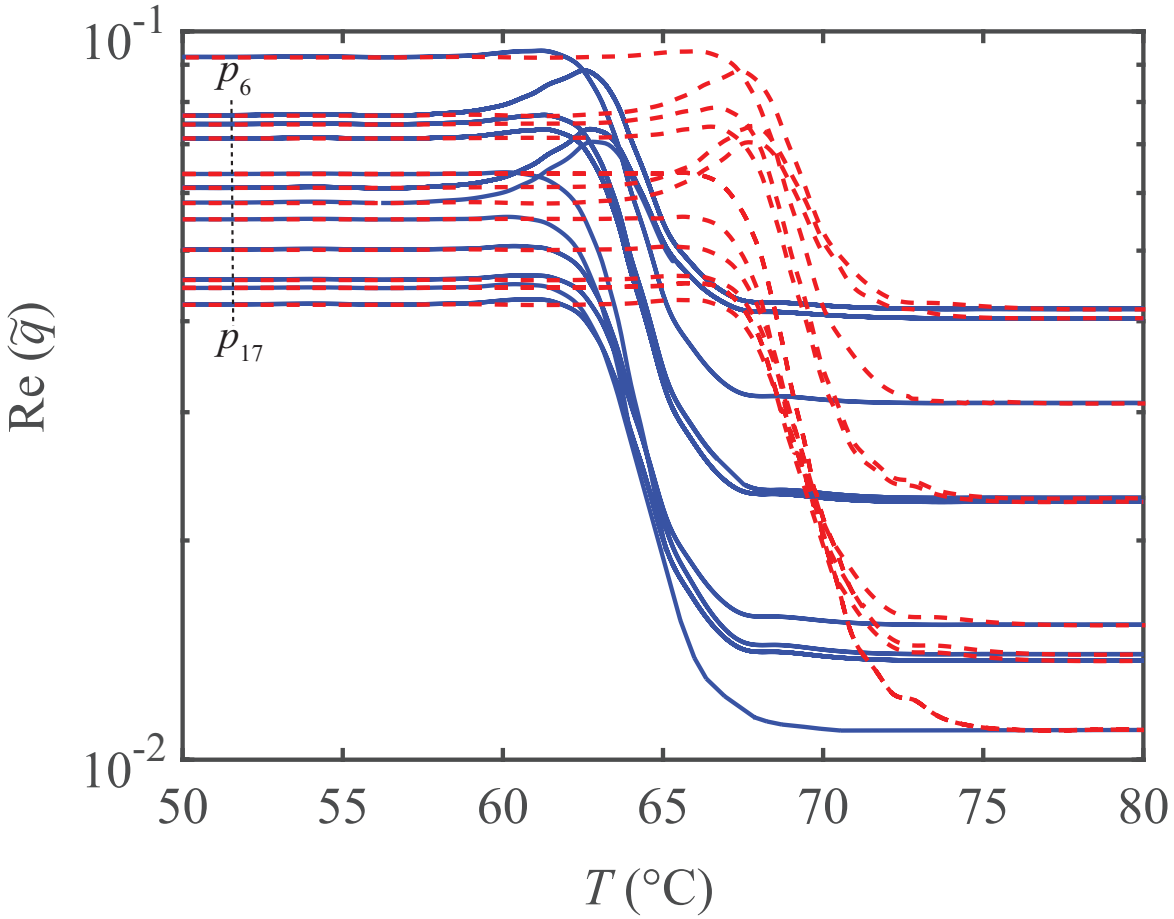

Figure 11: As Fig. 3 but for 0.01 <Re($\tilde{q}$)< 0.1 at $T = 50$ °C.

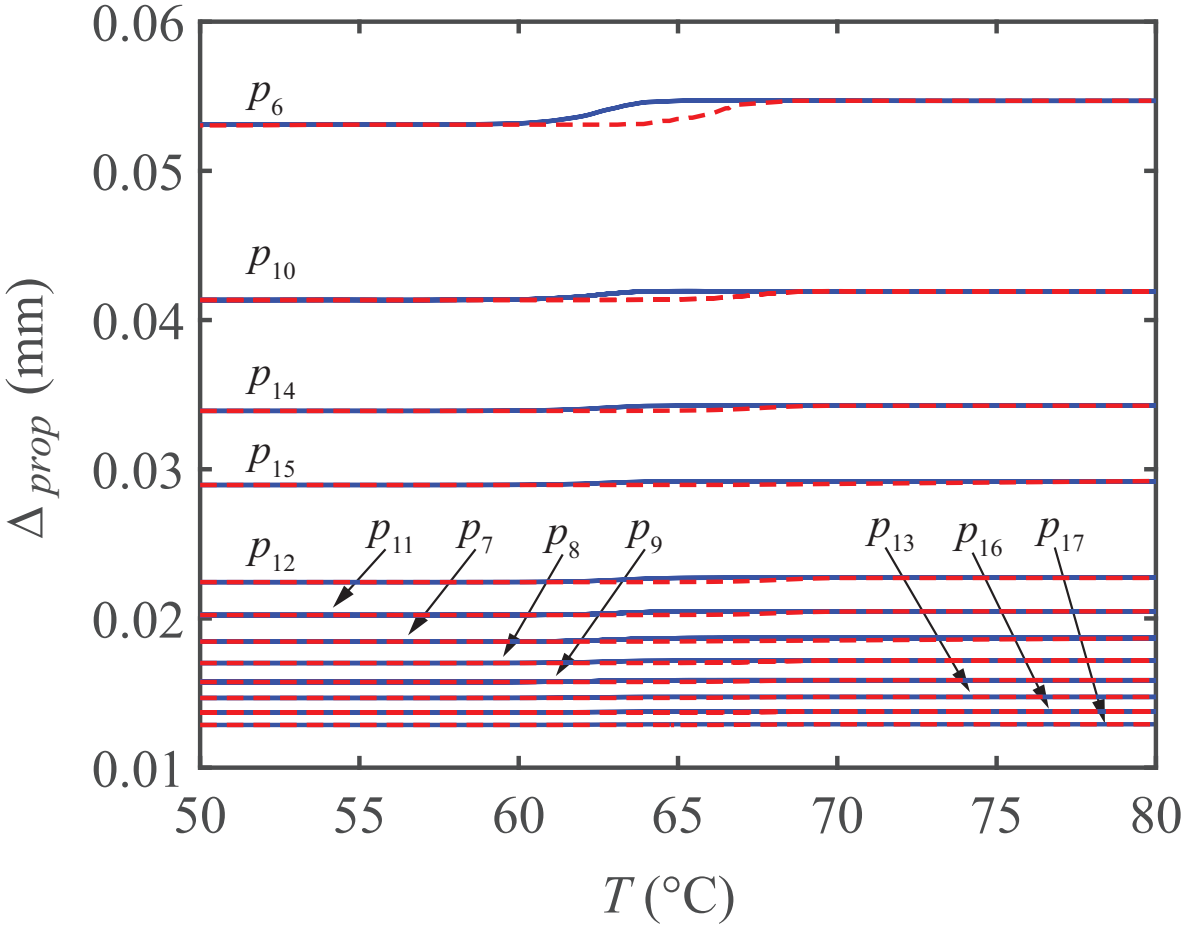

Figure 12: As Fig. 4 but for 0.01 <Re($\tilde{q}$)< 0.1 at $T = 50$ °C.

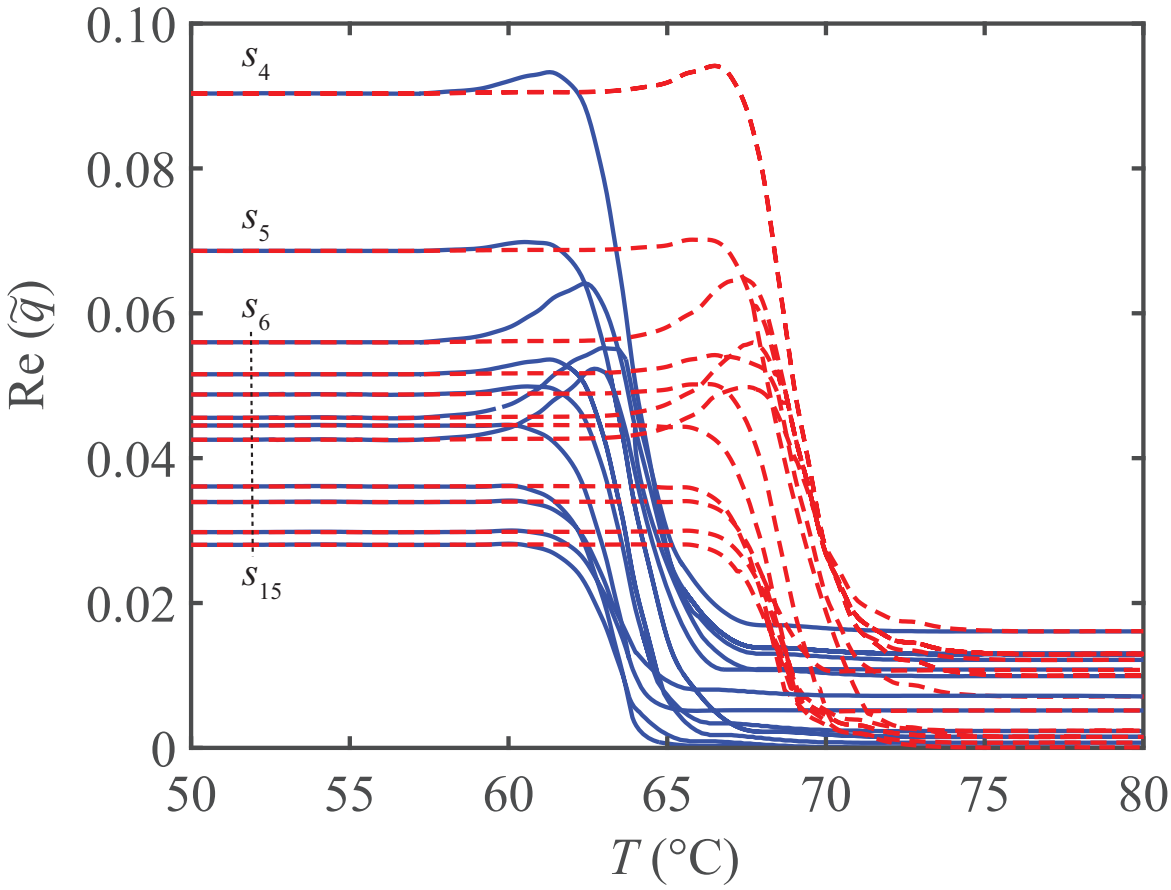

Figure 13: As Fig. 5 but for 0.01 <Re($\tilde{q}$)< 0.1 at $T = 50$ °C.

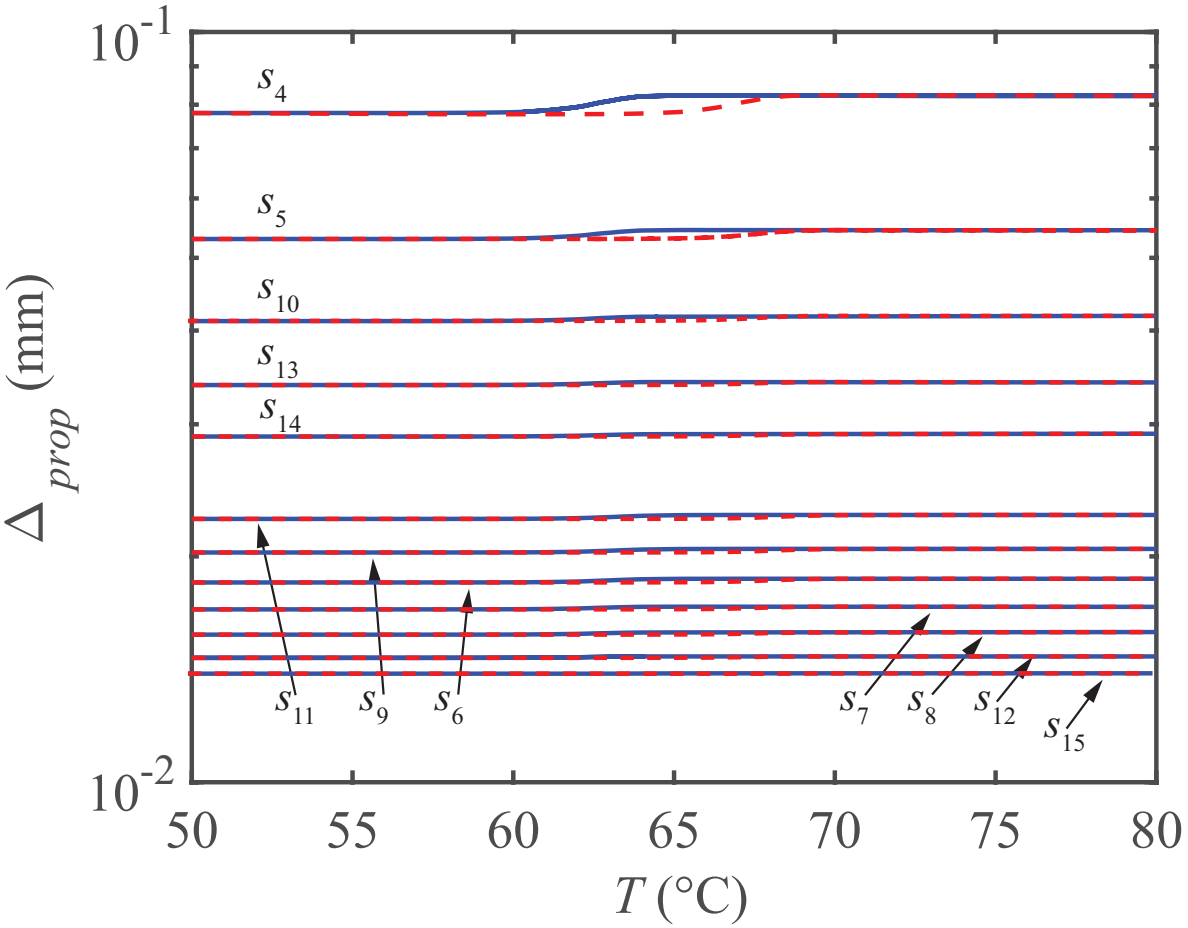

Figure 14: As Fig. 6 but for 0.01 <Re($\tilde{q}$)< 0.1 at $T = 50$ °C.